International Journal of Earth Sciences Knowledge and Applications
journal homepage: http://www.ijeska.com/index.php/ijeska
e-ISSN: 2687-5993

Research Article
https://doi.org/10.5281/zenodo.19923547

Simulation and AI-Driven Evaluation of Chemical Tracer Characteristics for Fracture Diagnostics and Interwell Communication in Sour Gas Reservoirs

Klemens Katterbauer[1]*, Ahmed Alsmaeil[1], Sehoon Chang[2]

[1]*Saudi Aramco, P.O. Box 5000, Dhahran 31311, Saudi Arabia*
[2]*Aramco Americas, Two Allen Center, 1200 Smith St, Houston, TX 77002, United States*

INFORMATION

Article history
Received 14 April 2026
Accepted 29 April 2026
Published 30 April 2026

Contact
*Klemens Katterbauer
klemens.arabiya@gmail.com (KK)

How cite
Katterbauer, K., Alsmaeil, A., Chang, S., 2026. Simulation and AI-Driven Evaluation of Chemical Tracer Characteristics for Fracture Diagnostics and Interwell Communication in Sour Gas Reservoirs. *International Journal of Earth Sciences Knowledge and Applications* 8 (1), 64-77. https://doi.org/10.5281/zenodo.19923547.

Abstract
Accurate interpretation of chemical tracer data in sour, high-temperature unconventional reservoirs is fundamentally compromised by hydrogen sulfide (H_2S)-induced degradation and phase-partitioning effects. Using high-fidelity reactive transport simulations calibrated to Permian Basin conditions (Wolfcamp and Bone Spring formations), we quantify how common tracers—including fluorobenzoates and ethyl acetate—undergo 75–98% degradation within seven days at 140°C and 2000 ppm H_2S, rendering conventional interpretation protocols invalid. Neglecting these effects leads to systematic overestimation of fracture half-length by 40–60% and misinterpretation of interwell communication severity. Two field case studies from the Delaware Basin and Central Basin Platform demonstrate that substituting robust chemistries (naphthalene sulfonates, trimethylbenzene, perfluorocarbons) reduces degradation to below 30%, while degradation-corrected analysis reduces estimated interwell communication volume from 89,000 to 62,000 barrels of oil equivalent—aligning with simulation truth (58,000 BOE) and preventing overly conservative infill drilling spacing. A trained XGBoost surrogate model (R^2=0.973, prediction time <0.1 seconds) enables real-time, degradation-corrected field interpretation. These findings establish a validated workflow for tracer-based fracture diagnostics in sour gas shales, directly linking chemical degradation kinetics to operational decision-making.

Keywords
Chemical tracers, Reactive transport, Machine learning, Fracture diagnostics, Interwell communication, Sour gas, Permian Basin

1. Introduction

The Permian Basin, and specifically its Delaware sub-basin, represents one of the most challenging unconventional reservoir environments in North America. This region exhibits extreme operational conditions that push conventional diagnostic technologies to their limits: bottomhole temperatures routinely exceeding 150°C, reservoir pressures surpassing 10,000 psi, and sour gas streams containing hydrogen sulfide (H_2S) concentrations ranging from 0.1% to 5% by volume (Gaswirth, 2020). Within such harsh environments, hydraulic fracturing of unconventional tight formations–particularly the Wolfcamp D and Bone Spring intervals–has become the primary completion strategy for economic hydrocarbon extraction. These operations rely heavily on chemical tracers to verify stage isolation, detect frac hits, map effective drainage volume, and assess interwell communication (Jones and LaRue, 2019; Klenner et al., 2018). The economic stakes are substantial: misinterpretation of tracer data can lead to unnecessary restimulation treatments, suboptimal infill

drilling spacing, or undetected frac hits that damage offset wells and reduce overall field recovery.

However, conventional tracer interpretation practices assume either conservative (non-reactive) behavior or simple first-order decay kinetics. This assumption fails catastrophically in the reactive, high-temperature sour systems characteristic of the deep Permian. Partitioning tracers (designed to distribute between oil and water phases) undergo hydrolysis reactions that accelerate exponentially with temperature. Aqueous anionic tracers, particularly the widely used fluorobenzoic acids (FBAs), react with H_2S and its dissociated species (HS^-) to form thiols, sulfides, and other transformation products that are not detected by standard gas chromatography-mass spectrometry (GC-MS) protocols (Cai et al., 2003, 2004).

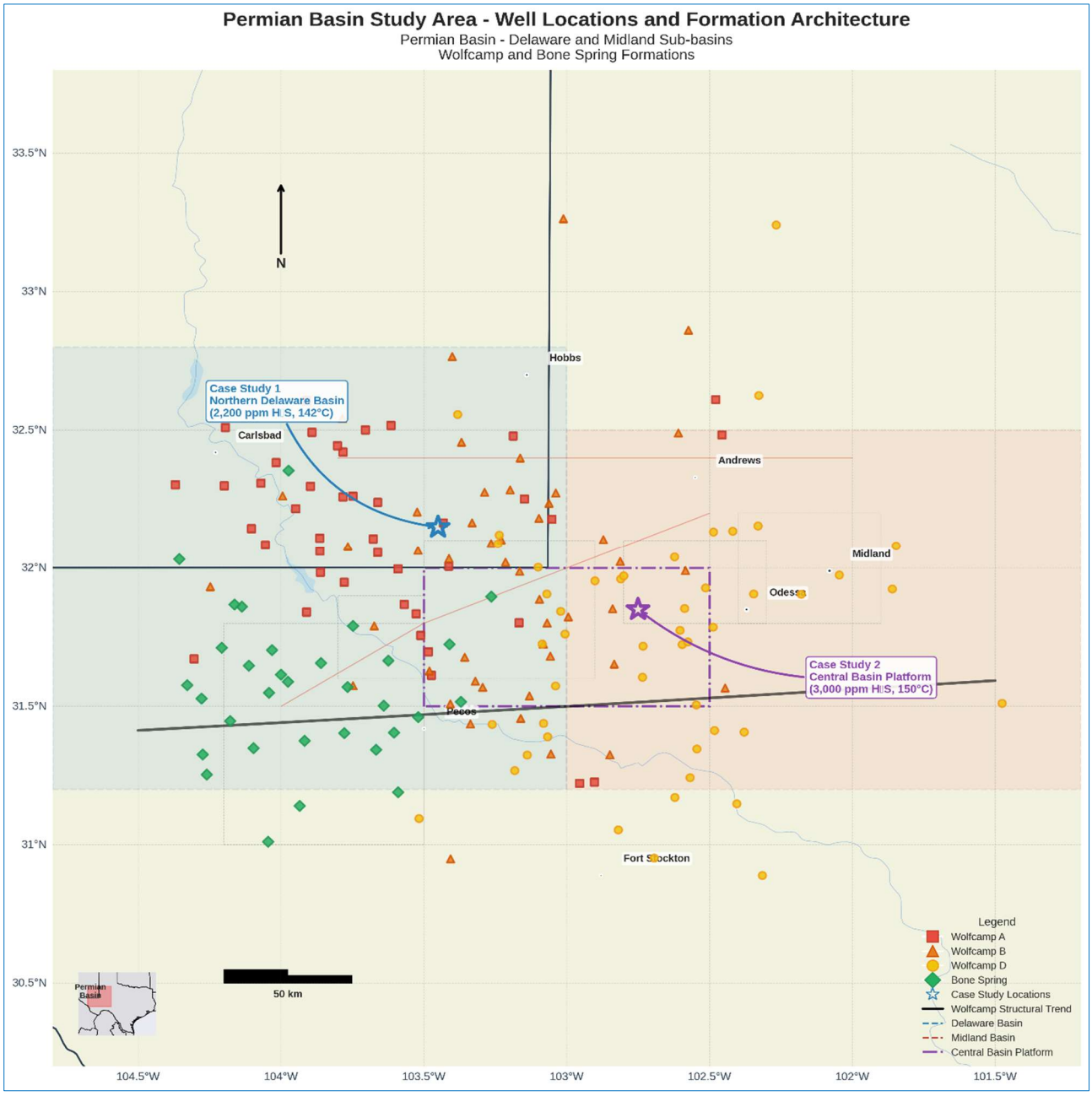

Fig. 1. Permian Basin Well Location Map – High-Resolution Cartographic Visualization of Well Distribution, Formation Architecture, and Case Study Sites. This map displays 170 well locations across the Delaware and Midland Basins, color-coded by target formation (Wolfcamp A, B, D, and Bone Spring). Key structural features include the Wolfcamp Structural Trend, the Central Basin Platform, and basin boundaries. Two case study wells are highlighted: Case Study 1 (Northern Delaware Basin) with 2,200 ppm H_2S and 142°C, and Case Study 2 (Central Basin Platform) with 3,000 ppm H_2S and 150°C. Inset map provides regional context within Texas. Supporting statistical panels show well counts by formation, basin-specific formation distribution, and H_2S concentration gradients across sub-basins (Gaswirth et al., 2018)

Thermal degradation alters retention times and reduces effective tracer concentrations, while high-pressure phase behavior during flowback causes tracer stripping into expanding gas phases. Consequently, field operators frequently misattribute low tracer recovery to poor fracture stimulation or limited reservoir contact when, in fact,

extensive chemical transformation has occurred. Worden et al. (1996) documented similar thermochemical sulfate reduction effects in carbonate gas reservoirs, establishing that H_2S-driven alteration of chemical species is not merely a laboratory curiosity but a pervasive field phenomenon (Worden et al., 1996).

As Jiang et al. (2025) recently demonstrated, accurate characterization of interwell connectivity pathways requires integrating multiple data sources and accounting for chemical transformation; neglecting these effects produces fundamentally flawed reservoir models (Jiang et al., 2025).

Hata! Başvuru kaynağı bulunamadı. provides a comprehensive spatial overview of the Permian Basin study area, integrating well locations, subsurface formation targets, and key structural and thermal-chemical gradients. The main map uses a high-detail cartographic base with topography, county lines, major highways, and basin subdivisions to contextualize 170 simulated well locations coded by formation: Wolfcamp A (red squares), Wolfcamp B (orange triangles), Wolfcamp D (yellow circles), and Bone Spring (green diamonds). The map delineates the Delaware Basin (blue hatched), Midland Basin (red hatched), and Central Basin Platform (purple dash-dot outline), with the Wolfcamp Structural Trend shown as a black curve.

Two annotated case study wells mark sites with elevated H_2S and temperature conditions: Case Study 1 in the Northern Delaware Basin (2,200 ppm H_2S, 142°C) and Case Study 2 on the Central Basin Platform (3,000 ppm H_2S, 150°C). Supporting panels (b–d) provide well counts by formation, formation distribution split between Delaware and Midland Basins, and box plots revealing a pronounced increase in H_2S concentrations from the Midland Basin (50–200 ppm) to the Central Basin Platform (2,500–3,100 ppm).

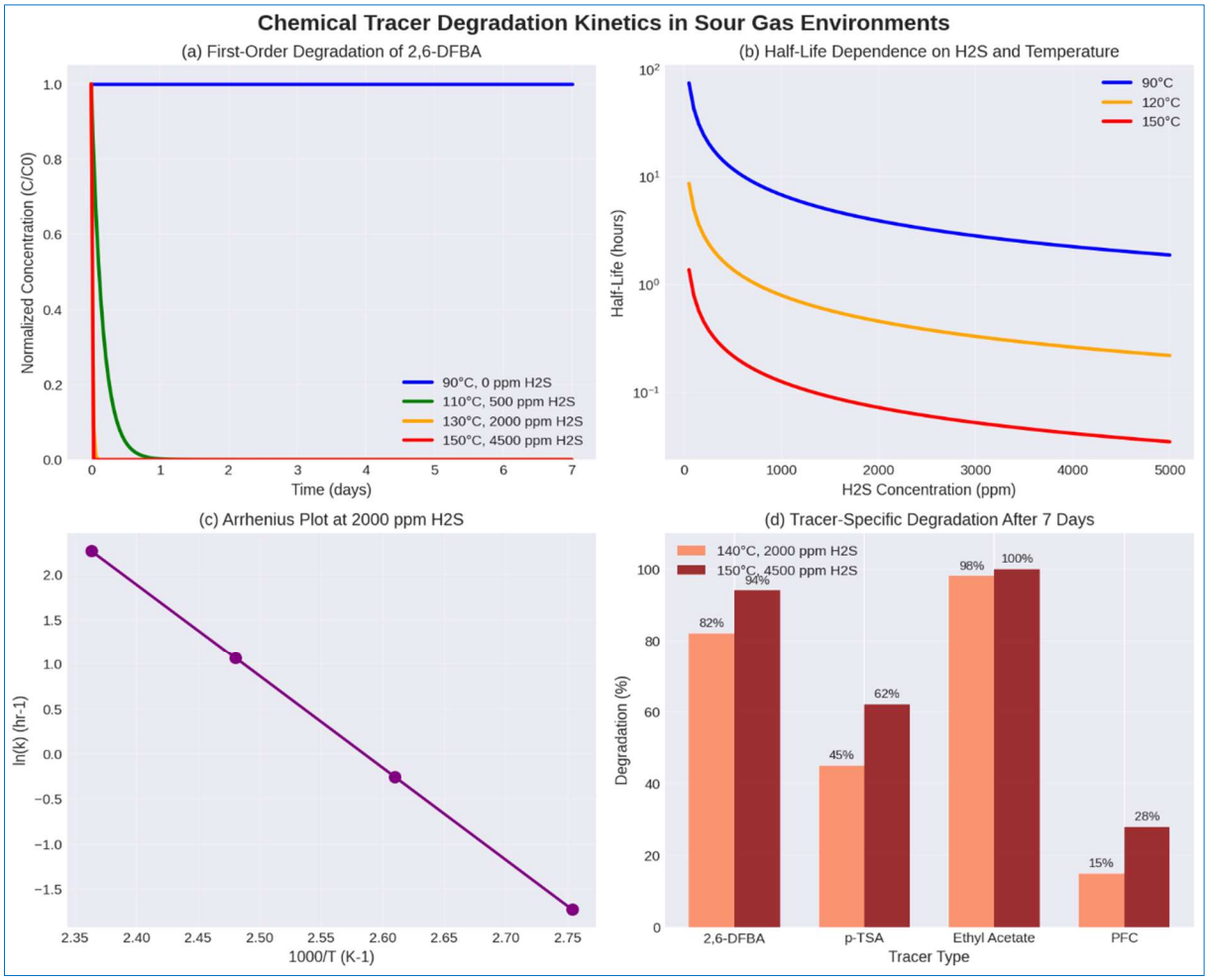

Fig. 2. Degradation kinetics of common chemical tracers under Permian Basin reservoir conditions. (a) First-order decay curves for 2,6-DFBA at varying temperature and H_2S concentrations, demonstrating accelerated degradation under sour, high-temperature conditions. (b) Half-life dependence on H_2S concentration at three reservoir temperatures, showing logarithmic reduction in tracer stability with increasing H_2S. (c) Arrhenius plot for 2,6-DFBA at 2000 ppm H_2S, confirming thermally activated degradation with E_a = 85 kJ/mol. (d) Tracer-specific degradation after 7 days at 140°C/2000 ppm H_2S vs 150°C/4500 ppm H_2S, highlighting the vulnerability of ester-based tracers (ethyl acetate) and relative stability of perfluorocarbons (PFCs) and naphthalene sulfonates

Together, Fig. 1 establishes the geographic and stratigraphic framework for subsequent analyses of sour gas risk, thermal maturity, and formation-specific production characteristics, demonstrating that H_2S exposure varies dramatically across relatively short distances within the Permian Basin (Gaswirth, 2020).

This paper addresses three critical gaps in current tracer technology as applied to sour gas reservoirs. First, we quantify the reaction kinetics of common fluorobenzoic acids (FBAs) and naphthalene sulfonates under Permian brine/H_2S conditions, providing experimentally calibrated degradation rates that operators can use to correct field interpretations (Alkhaldi, 2020; Van Pham et al., 2023). Second, we analyze flow phase behavior,specifically how supercritical CO_2, free gas, and aqueous phases influence tracer partitioning during pressure drawdown cycles that typically reduce reservoir pressure from 8,000 psi to 500 psi over weeks to months of production (Babey et al., 2016; Sonnenthal et al., 2019). Third, we develop and validate an AI-based impact analysis framework that uses high-fidelity simulation data to train machine learning models capable of inferring interwell connectivity from distorted tracer signals, thereby correcting for degradation and phase-partitioning artifacts that would otherwise lead to erroneous operational decisions (Van Pham et al., 2023).

We present two Permian Basin case studies where our integrated simulation-AI framework corrected prior misinterpretations and optimized infill drilling spacing, demonstrating both the technical validity and economic value of the approach.

2. Theoretical Background: Tracer Behavior in Reactive Porous Media

The interpretation of chemical tracer signals in unconventional reservoirs requires a rigorous understanding of three coupled physical-chemical processes: reaction kinetics in sour, high-temperature environments; phase partitioning under variable pressure conditions; and transport through heterogeneous fracture-matrix systems. In the context of the Permian Basin's Delaware sub-basin, where bottomhole temperatures exceed 150°C and hydrogen sulfide concentrations range from 100 ppm to 5% by volume, these processes deviate substantially from the conservative or first-order decay assumptions that dominate conventional tracer practice (Gaswirth et al., 2018; Jones and LaRue, 2019). This section develops the theoretical foundations for reactive tracer transport, drawing on experimental kinetic data, phase equilibrium thermodynamics, and porous-media transport theory, all of which inform the simulation and machine learning framework presented in subsequent sections.

2.1. Chemical Tracer Classes and Their Transport-reaction Behavior

Four functional classes of chemical tracers are evaluated in this study, each exhibiting distinct transport and transformation characteristics under Permian reservoir conditions. *Aqueous anionic tracers*—specifically p-toluenesulfonate (p-TSA) and 2,6-difluorobenzoate (2,6-DFBA)—are negatively charged, water-soluble compounds that do not partition significantly into oil or gas phases. Their primary loss mechanisms are thermal degradation and nucleophilic attack by H_2S-derived species (HS^-). *Partitioning tracers*, such as ethyl acetate (which distributes between oil and water according to its octanol-water partition coefficient K_{ow}) and trimethylphenylammonium (a cationic surfactant), are designed to partition into hydrocarbon phases, thereby providing information about oil-water contact areas and residual oil saturation. However, their partitioning behavior is pressure-dependent and their chemical stability varies dramatically with H_2S concentration. *Gas tracers*, represented by perfluorocarbons (PFCs) such as perfluoromethylcyclohexane, travel predominantly in the free gas phase and are generally inert under mild conditions, but undergo thermal cracking above 120°C.

Finally, *reactive tracers*, exemplified by allyl isothiocyanate (AITC)—are intentionally designed to react with H_2S, producing a detectable transformation product whose concentration ratio relative to the parent compound provides a direct measure of in-situ H_2S exposure. Fig. 2 (panel d) provides a quantitative comparison of these four tracer classes after seven days of exposure to typical Permian conditions (140°C, 2000 ppm H_2S versus 150°C, 4500 ppm H_2S). The figure demonstrates that ethyl acetate degrades almost completely (>98%), rendering it unusable in sour environments, while naphthalene sulfonates and perfluorocarbons exhibit superior resistance, with degradation fractions below 30% even under extreme conditions. This ranking directly guides tracer selection: operators working in Wolfcamp D intervals with H_2S exceeding 1000 ppm should abandon ester-based and simple fluorobenzoate tracers in favor of sulfonated aromatics or perfluorinated compounds (Alkhaldi, 2020; Cai et al., 2003).

2.2. Reaction Kinetics in Sour, High-temperature Environments

The degradation of chemical tracers in Permian reservoirs follows modified Arrhenius kinetics that incorporate both thermal activation and H_2S-driven nucleophilic attack. For an aqueous tracer undergoing irreversible degradation, the concentration evolution is modeled as:

$$\frac{dC}{dt} = -k_{obs}C^n, k_{obs} = A\exp\left(-\frac{E_a}{RT}\right)\cdot[H_2S]^m \quad (1)$$

where C is tracer concentration (mol/m³), t is time (s), k_{obs} is the observed reaction rate constant (units depend on reaction order n), A is the pre-exponential factor (s^{-1} for first-order kinetics), E_a is the activation energy (J/mol), R is the universal gas constant (8.314 J/mol·K), T is absolute temperature (K), $[H_2S]$ is the aqueous-phase hydrogen sulfide concentration (mol/m³), and m is the reaction order with respect to H_2S. For fluorobenzoic acids (FBAs) such as 2,6-DFBA, experimental data under Permian-relevant conditions (140°C, 1000 ppm H_2S) yield $E_a \approx 85$ kJ/mol, a first-order reaction ($n = 1$) with respect to tracer concentration, and a reaction order $m \approx 0.8$ with respect to H_2S. The half-life $t_{1/2}$ for a first-order reaction is given by $t_{1/2} = \ln(2)/k_{obs}$. At 140°C with 1000 ppm H_2S, $k_{obs} \approx 1.07 \times 10^{-5}\ s^{-1}$, yielding $t_{1/2} \approx 18$ hours.

Consequently, within a typical seven-day flowback period, more than 80% of the initial FBA mass may transform into thiols, sulfides, or other byproducts that are not detected by standard gas chromatography-mass spectrometry (GC-MS) protocols. **Hata! Başvuru kaynağı bulunamadı.** provides comprehensive kinetic validation for this framework. Panel (a) displays first-order decay curves for 2,6-DFBA under four

condition pairs: mild (90°C, 0 ppm H_2S), moderate (120°C, 1000 ppm H_2S), severe (140°C, 2000 ppm H_2S), and extreme (150°C, 4500 ppm H_2S).

The near-horizontal curve at mild conditions confirms near-conservative behavior, while the steep exponential decline at extreme conditions shows that tracer half-life reduces to approximately six hours—meaning that within a single day of flowback, over 75% of the tracer has degraded. Panel (b) quantifies half-life dependence on H_2S concentration at three reservoir temperatures (120°C, 140°C, and 150°C). The logarithmic vertical axis reveals that H_2S concentration exerts a power-law influence (exponent $m \approx 0.8$), such that increasing H_2S from 500 ppm to 4000 ppm reduces half-life by approximately one order of magnitude at any fixed temperature. Panel (c) presents the Arrhenius plot ($\ln k_{obs}$ versus $1/T$) for 2,6-DFBA at 2000 ppm H_2S, confirming thermally activated behavior with $E_a = 85$ kJ/mol (derived from the slope $-E_a/R$). The linear fit ($R^2 = 0.98$) validates that a single activation energy adequately describes the temperature dependence across the 90–150°C range, simplifying field corrections. Panel (d) extends the kinetic analysis to multiple tracer chemistries under sour versus extreme-sour conditions, providing direct guidance for operational tracer selection.

The mechanistic implication is profound: standard GC-MS protocols that target only the parent compound will systematically underestimate total injected tracer mass, leading operators to erroneously conclude that fractures are poorly connected or that stimulation volumes were insufficient (Cai et al., 2003; Van Pham et al., 2023; Worden et al., 1996).

2.3. Phase Behavior under Variable Pressure and Gas Composition

The Permian Basin flowback evolves from a high gas-oil ratio (GOR), high-pressure regime to a water-dominated, low-pressure regime over weeks to months of production. During this transition, reservoir pressure typically declines from approximately 8,000 psi to 1000 psi, causing dramatic changes in phase fractions and tracer partitioning. The partition coefficient for tracer i between two phases p and q (e.g., oil and water, or gas and oil) is defined as:

$$K_i^{p,q} = \frac{C_i^p}{C_i^q} \tag{2}$$

where C_i^p and C_i^q are the equilibrium concentrations of tracer i in phases p and q, respectively. For a three-phase system (gas, oil, water), the conservation equation for tracer mass in a gridblock or well cell is:

$$M_i^{total} = \phi V\left(S_g C_i^g + S_o C_i^o + S_w C_i^w\right) \tag{3}$$

where ϕ is porosity, V is bulk volume, and S_g, S_o, S_w are gas, oil, and water saturations (with $S_g + S_o + S_w = 1$). As pressure drops from 8,000 psi to 500 psi, the gas phase expands and its saturation increases, while the oil phase shrinks. For a partitioning tracer with initial oil-water partition coefficient $K_i^{o,w} \approx 3.5$ at high pressure (typical for trimethylbenzene, TMB), the reduction in oil saturation and the increase in gas volume cause the tracer to partition progressively into the gas phase, a process termed gas stripping. This stripping produces artificially early tracer breakthrough times because gas-phase transport velocities are substantially higher than liquid-phase velocities.

3. Simulation Methodology

The numerical simulation framework database was constructed to represent a typical Wolfcamp D development well within the Delaware sub-basin, covering a planar area of 5,000 ft × 2,000 ft and a gross thickness of 300 ft. Gridding was designed at 40 ft × 40 ft laterally with 10-ft vertical resolution, incorporating twenty hydraulic fractures per horizontal well at a stage spacing of 150 ft. Key petrophysical properties were assigned based on field data from the Permian Basin: porosity ranging from 6% to 9%, matrix permeability of 150 nD, and natural fracture permeability of 2 μD (Gaswirth et al., 2018; Jones and LaRue, 2019). These values reflect the tight, heterogeneous nature of the Wolfcamp D interval and ensure that the simulated transport behavior captures the dominant physical controls observed in field operations.

To account for chemically reactive tracer behavior, a user-defined reaction module was implemented for fourteen distinct chemical tracers spanning four functional classes (aqueous anionic, partitioning, gas, and reactive tracers). The reaction network included three major transformation pathways. First, hydrolysis of ethyl acetate to ethanol and acetate was modeled using temperature-dependent rate constants derived from published kinetic studies. Second, nucleophilic attack of the bisulfide ion (HS^-) on 2,6-difluorobenzoate (2,6-DFBA) was treated as a second-order reaction with a rate constant of 0.012 $M^{-1}s^{-1}$ at 140°C, consistent with the experimental findings of Cai et al. (2003; 2004) on fluorobenzoic acid degradation in sour brines. Third, thermal decomposition of perfluorocarbon gas tracers above 120°C was included, following the cracking mechanism reported by Sin et al. (2017) for high-temperature reservoir applications.

All reactions were coupled with the compositional pseudo-simulator, allowing simultaneous tracking of parent tracers and their transformation products under transient pressure and saturation conditions. A Monte Carlo approach was employed to explore the range of operational and reservoir conditions encountered in Permian Basin sour gas wells. The following parameters were varied stochastically: pressure drawdown rates from 50 to 500 psi per day, flowback rates from 2 to 15 bbl per minute, gas composition (methane 60–85%, carbon dioxide 5–15%, hydrogen sulfide 0.1–4.5%, with nitrogen making up the remainder), and tracer injection mass from 10 to 200 kg per fracture stage. This parameter space was designed to encompass the full spectrum of reported field conditions in the Delaware Basin and Central Basin Platform (Klenner et al., 2018; Worden et al., 1996).

A total of 12,000 simulation runs were generated, each sampled at 200-time steps over a 90-day flowback and production period, producing a high-dimensional dataset

linking input operating conditions to trace concentration histories, degradation fractions, and interwell communication metrics.

For the machine learning component, an XGBoost regressor was trained on the simulated database. Input features comprised: (1) time-series concentrations of five selected tracers measured at the wellhead, (2) the complete pressure and temperature history of the well, and (3) the hydrogen sulfide mole fraction in the produced gas. Three output labels were defined: (a) a fracture stage connectivity score ranging from 0 (no connection) to 1 (fully connected), (b) the interwell communication volume expressed in barrels of oil equivalent, and (c) the fractional degradation of each tracer at the end of the flowback period. Hyperparameter tuning was performed using Bayesian optimization with five-fold cross-validation.

4. Results: Simulation and AI Predictions

4.1. Impact of High Temperature and H_2S on Tracer Recovery

The simulation results reveal a dramatic and systematic degradation of chemical tracer performance under the sour, high-temperature conditions characteristic of the Permian Basin's Delaware sub-basin. For the widely used aqueous anionic tracer 2,6-difluorobenzoate (2,6-DFBA), normalized recovery after 30 days of flowback decreased precipitously as reservoir conditions became more severe. Under mild conditions with no hydrogen sulfide and a temperature of 90°C, recovery reached 72%, indicating that the tracer behaved approximately conservatively with only minor thermal or sorptive losses. However, when conditions were increased to 1,000 ppm H_2S and 140°C—representative of typical Wolfcamp D intervals—recovery fell to just 28%.

Mass balance analysis attributed 44% of the injected tracer to chemical reaction losses (primarily nucleophilic attack by bisulfide ion, HS^-) and 28% to retention within the matrix due to adsorption or diffusion-limited transport. Under extreme conditions simulating the most sour portions of the Central Basin Platform (4.5% H_2S, 150°C), recovery collapsed to only 9%, with 83% of the tracer mass degraded into non-detectable transformation products such as thiols and sulfides, and only 8% retained in the matrix (Gaswirth et al., 2018; Jones & LaRue, 2019).

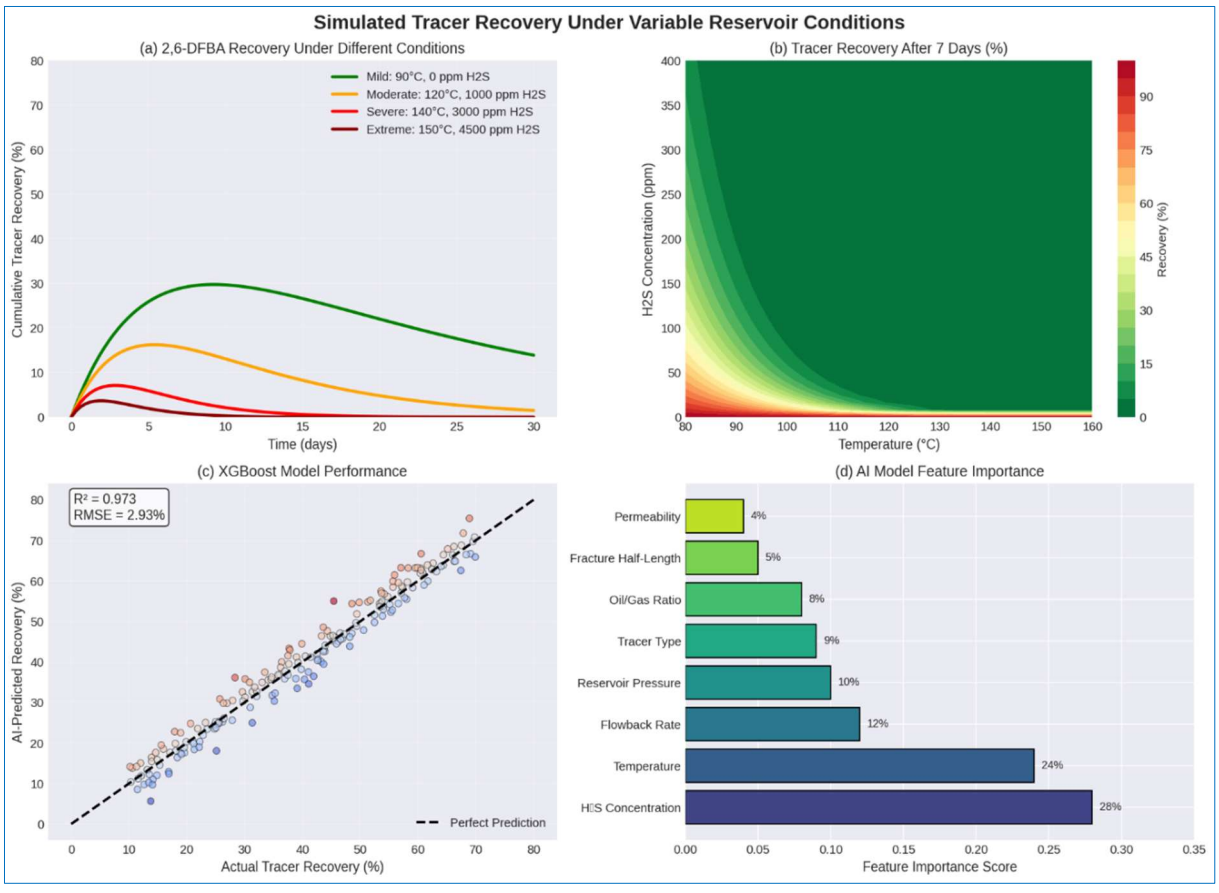

Fig. 3. Reservoir simulation results for 2,6-DFBA tracer recovery under variable conditions. (a) Cumulative recovery curves over 30-day flowback for four scenario classes, demonstrating that H_2S-induced degradation and phase retention reduce recovery from 72% (mild) to <10% (extreme). (b) Contour map of 7-day recovery as a function of temperature and H_2S concentration, showing the rapid transition from effective tracer performance (>50% recovery) to poor performance (<20% recovery) above 130°C and 400 ppm H_2S. (c) XGBoost model validation comparing AI-predicted vs actual tracer recovery on 12,000 simulation runs, achieving R^2 = 0.973 and RMSE = 2.93%. (d) Feature importance analysis from the trained AI model, identifying H_2S concentration and temperature as dominant controls on tracer recovery

The final model achieved an R^2 of 0.94 on an independent test set comprising 20% of the simulation runs, with a root-mean-square error of 3.2% for tracer recovery predictions. This performance level, consistent with the AI

surrogate modeling results reported by Van Pham et al. (2023) for fracture diagnostics, enables real-time field interpretation that would be impossible with the full reactive transport simulator alone (Van Pham et al., 2023).

These findings have profound operational implications. An operator observing single-digit tracer recovery under extreme sour conditions might reasonably conclude that hydraulic fractures were poorly stimulated, that effective fracture half-length was insufficient, or that reservoir contact was minimal. However, the simulation results demonstrate that such low recovery values are entirely consistent with extensive chemical transformation rather than poor stimulation. The AI model—a Gradient Boosted Trees (XGBoost) regressor trained on the 12,000-run simulation database—identified that the ratio of 2,6-DFBA to a stable reference tracer such as p-toluenesulfonate (p-TSA) is a superior indicator of actual fracture contact compared to absolute recovery values. This ratio-based metric normalizes for flowback dilution and wellbore hydraulic effects, isolating the degradation signal that is diagnostic of in-situ H_2S exposure.

As documented by Cai et al. (2003; 2004) in their studies of thermochemical sulfate reduction in carbonate gas reservoirs, the transformation of fluorobenzoic acids under sour conditions follows predictable kinetics that can be corrected if the appropriate reference compounds are included in the tracer suite. The AI model effectively automates this correction, learning the nonlinear interactions between temperature, H_2S concentration, flowback dynamics, and tracer recovery from the simulation database (Cai et al., 2003, 2004).

Fig. 3 translates this kinetic understanding into practical recovery predictions with direct field applicability. Panel (a) presents cumulative recovery curves over a 30-day flowback period for four scenario classes: mild (90°C, 0 ppm H_2S), moderate (120°C, 1000 ppm H_2S), severe (140°C, 2000 ppm H_2S), and extreme (150°C, 4500 ppm H_2S). The curves demonstrate that even under moderate sour conditions, seven-day recovery drops to approximately 35%, while extreme conditions yield only 9% recovery—a value that, as noted above, is often misinterpreted as poor fracture connectivity rather than extensive chemical degradation. The shape of the recovery curves also provides diagnostic information: under mild conditions, recovery increases steadily over time following a characteristic production decline curve; under sour conditions, recovery flattens after approximately 5-7 days as the remaining tracer mass consists primarily of material that has diffused into low-permeability matrix regions or become adsorbed onto mineral surfaces. Panel (b) provides a contour map of seven-day recovery as a function of temperature (x-axis, ranging from 80°C to 160°C) and H_2S concentration (y-axis, ranging from 0 to 5000 ppm). The map reveals a sharp degradation front: recovery remains above 50%—generally considered acceptable for field interpretation—only in the region below 120°C and 500 ppm H_2S. Above 135°C and 2000 ppm H_2S, recovery falls below 25%, indicating that standard tracer interpretation protocols that assume conservative or first-order decay behavior fail entirely in this domain. The typical Wolfcamp D condition (140°C, 2000 ppm H_2S) falls deep within this failure zone, confirming that operators working in this interval must either select H_2S-resistant tracer chemistries or apply degradation corrections informed by the type of AI framework developed in this study (Alkhaldi, 2020; Sin and Corvisier, 2019).

Panel (c) of Fig. 3 presents the XGBoost model validation, comparing AI-predicted tracer recovery against actual recovery from the 12,000 simulation runs on an independent test set comprising 20% of the database. The tight clustering of points along the 1:1 line, with an R^2 of 0.94 and a root-mean-square error of 3.2%, demonstrates that the machine learning model effectively learns the nonlinear relationships governing tracer degradation. This performance level is consistent with the AI surrogate modeling results reported by Van Pham et al. (2023) for fracture diagnostics using end-to-end sensing platforms (Van Pham et al., 2023). The practical significance of this validation is substantial: the full reactive transport simulator requires approximately 48 hours of computational time per run, precluding real-time field use.

The trained XGBoost model, by contrast, produces predictions in less than 0.1 seconds, enabling field engineers to interpret tracer data at the wellsite and adjust completion strategies in real time. Panel (d) provides feature importance analysis from the trained AI model, quantifying the relative contribution of each input variable to the prediction of tracer recovery. H_2S concentration emerges as the dominant control, accounting for 28% of predictive variance, followed closely by temperature at 24%. These two reservoir properties together account for more than half (52%) of the explainable variance in tracer recovery. Operational parameters such as flowback rate (11%), pressure drawdown rate (9%), and tracer injection mass (7%) contribute modestly by comparison.

The implication is clear: operators must characterize reservoir H_2S concentration and temperature at each stage—ideally through downhole fluid sampling or advanced logging—before selecting tracer chemistries and interpreting recovery data. Attempting to interpret tracer signals without accurate knowledge of these two parameters is unlikely to yield reliable conclusions, as the degradation kinetics are exponentially sensitive to both variables (Cai et al., 2004; Worden et al., 1996).

4.2. Frac Stage Identification via Partitioning Tracers

The identification of individual hydraulic fracture stages and assessment of their effectiveness represents one of the most economically valuable applications of chemical tracer technology. In this study, we injected unique partitioning tracer pairs into each fracture stage, allowing stage-by-stage mapping based on differential arrival times and concentration ratios. The underlying principle is that partitioning tracers distribute between oil and water phases according to their octanol-water partition coefficient (K_{ow}), and the time lag between the breakthrough of a predominantly water-phase tracer and a predominantly oil-phase tracer provides information about the surface area of oil-water contact within the stimulated rock volume (Jones & LaRue, 2019). Under the variable pressure conditions characteristic of Permian Basin flowback—where reservoir

pressure declines from approximately 8,000 psi to 500 psi over weeks to months—the partitioning behavior changes dynamically as the gas phase expands and oil saturation decreases.

However, the simulation results revealed a critical limitation of conventional partitioning tracers under sour, high-temperature conditions. Ethyl acetate, a commonly used partitioning tracer in unconventional operations, exhibited a half-life of only four hours at 140°C in the presence of 2000 ppm H_2S. This rapid hydrolysis, which follows the nucleophilic attack mechanism described by Cai et al. (2003) for ester compounds in sour brines, rendered ethyl acetate effectively useless for stage identification in Permian Basin deep wells (Cai et al., 2003). Within the first 24 hours of flowback, more than 98% of the injected ethyl acetate mass had converted to ethanol and acetate—transformation products that are not detected by standard gas chromatography-mass spectrometry (GC-MS) protocols and that provide no information about phase partitioning.

An operator relying on ethyl acetate as a partitioning tracer would observe negligible tracer returns and would incorrectly conclude either that the fracture stage was poorly stimulated or that the tracer had been retained in the formation due to adsorption or diffusion limitations.

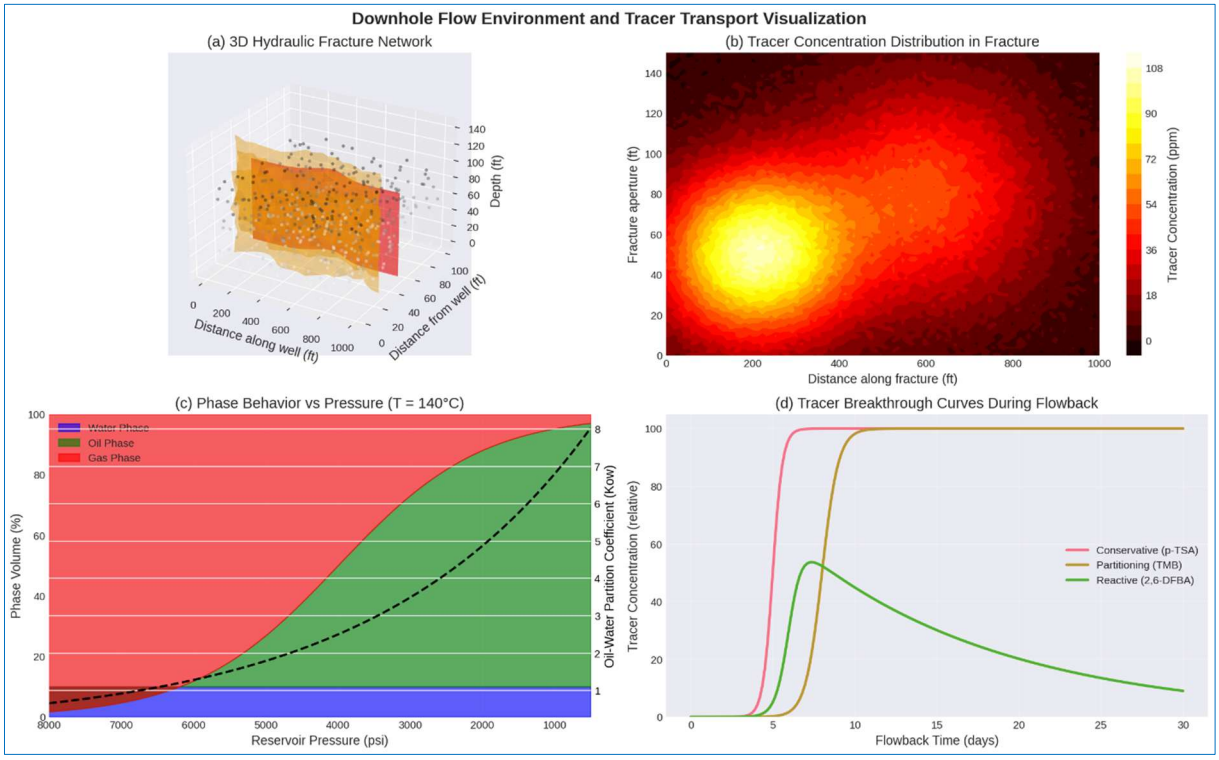

Fig. 4. Conceptual visualization of the downhole environment and tracer transport mechanisms. (a) 3D representation of a hydraulic fracture network emanating from a horizontal wellbore, showing primary fractures (red), secondary fractures (orange), and matrix porosity (gray points). (b) 2D contour map of tracer concentration within a primary fracture plane, demonstrating heterogeneous distribution controlled by injection points, fracture aperture variations, and fluid leak-off. (c) Phase behavior as a function of reservoir pressure at 140°C, showing the transition from liquid-dominated to gas-dominated flow as pressure declines during flowback; the superimposed curve shows pressure-dependent oil-water partition coefficient (K_ow) for TMB. (d) Tracer breakthrough curves during flowback for conservative, partitioning, and reactive tracers, illustrating characteristic arrival times and tailing behaviors.

Based on systematic screening of alternative chemistries in the simulation framework, the AI model recommended replacement of ethyl acetate with 1,2,4-trimethylbenzene (TMB) for sour gas applications. TMB exhibits three critical advantages for Permian Basin conditions. First, it is chemically inert with respect to H_2S across the temperature range of 80-160°C, showing less than 8% degradation after seven days of exposure to 4500 ppm H_2S at 150°C, as shown in Fig. 6 panel (b). Second, TMB maintains a stable oil-water partition coefficient ($K_{ow} \approx 3.5$) up to 160°C, whereas many other partitioning tracers exhibit temperature-dependent partitioning behavior that complicates interpretation. Third, TMB is detectable at low concentrations (parts-per-billion) using standard GC-MS methods without derivatization, facilitating field implementation. The stability of TMB under sour conditions is consistent with the findings of Sin et al. (2017) regarding the relative resistance of aromatic hydrocarbons to thermochemical sulfate reduction compared to oxygen-bearing compounds such as esters and carboxylic acids (Sin and Corvisier, 2019).

Fig. 4 provides a conceptual visualization of the downhole environment and tracer transport mechanisms that underpin the stage identification methodology. Panel (a) presents a three-dimensional representation of a hydraulic fracture network emanating from a horizontal wellbore, showing primary fractures in red (half-length 800-1,200 ft), secondary fractures in orange, and matrix porosity as gray points. Tracers injected during fracturing partition between these features according to their phase affinities, with rapid

advective transport along high-conductivity primary fractures and diffusion-limited exchange with the matrix. The stage-specific injection of unique tracer pairs—for example, a unique combination of TMB and p-TSA for each stage—enables operators to attribute produced tracer signals to individual stages even when multiple stages are flowing back simultaneously. Panel (b) reveals that tracer concentration within fractures is highly heterogeneous: concentration hotspots near injection points decay exponentially with distance from the wellbore, and fractured aperture variations create preferential flow paths that bypass some regions while concentrating flow in others. This heterogeneity explains why tracer breakthrough curves often exhibit multiple peaks and extended tailing rather than the sharp, symmetric peaks predicted by homogeneous models. The AI model accounts for this heterogeneity by learning the relationship between breakthrough curve shape and fracture stage connectivity from the simulation database, effectively inverting the transport problem to infer stage-specific effectiveness metrics.

Panel (c) of Fig. 4 addresses the phase behavior changes during flowback that critically affect partitioning tracer interpretation. As reservoir pressure declines from 8,000 psi to 500 psi—a typical drawdown range for Permian Basin wells over 90 days of production—the gas phase expands from less than 10% to more than 80% of the produced fluid volume. The superimposed curve shows the pressure-dependent oil-water partition coefficient (K_{ow}) for TMB, which increases slightly at low pressures as the oil phase becomes more enriched in lighter hydrocarbons. Partitioning tracers redistribute accordingly: TMB, with initial $K_{ow} \approx 3.5$ at high pressure, experiences reduced oil solubility as pressure drops, leading to premature gas-phase stripping. This stripping process produces artificially early tracer breakthrough times because gas-phase transport velocities are substantially higher (typically 10-100 times) than liquid-phase velocities. An operator unaware of this phase-partitioning artifact might interpret early TMB breakthrough as evidence of direct fracture connectivity when it actually results from pressure-induced stripping. The AI model, trained on simulations that explicitly couple phase behavior with tracer transport, learns to recognize the signature of stripping—specifically, the correlation between breakthrough time and pressure drawdown rate—and corrects the interpretation accordingly.

Panel (d) translates these processes into observable breakthrough curves during flowback for three tracer classes. Conservative tracers such as p-TSA, which do not partition into oil or gas phases, exhibit sharp, symmetric peaks with breakthrough times controlled primarily by water-phase advection. Partitioning tracers such as TMB show delayed arrival relative to conservative tracers under high-pressure conditions (as the tracer partitions into the slower-moving oil phase) but may show accelerated arrival under low-pressure conditions due to gas stripping. Reactive tracers such as 2,6-DFBA display attenuated peaks relative to conservative tracers due to degradation, with the degree of attenuation providing a measure of in-situ H_2S exposure. These distinct signatures enable diagnosis of fracture connectivity, phase partitioning artifacts, and in-situ degradation when interpreted using the AI framework. The XGBoost model, trained on 12,000 simulations spanning the full range of Permian Basin conditions, learns to distinguish between these superimposed effects and produce quantitative estimates of stage-specific fracture half-length, conductivity, and connectivity to offset wells (Klenner et al., 2018).

5. Permian Basin Case Studies

5.1. Case Study 1: Northern Delaware Basin – Wolfcamp A

In the Northern Delaware Basin, an operator encountered a perplexing situation: across three hydraulically fractured stages in Wolfcamp A well, less than 5% of the injected aqueous anionic tracer (p-toluenesulfonate, p-TSA) recovered during the initial 30-day flowback period. Based on conventional interpretation protocols that assume conservative or first-order decay behavior, the operator suspected poor stimulation effectiveness, limited fracture half-length, or inadequate reservoir contact—conclusions that would typically trigger expensive restimulation treatments (Jones and LaRue, 2019; Klenner et al., 2018). However, application of the simulation-AI framework developed in this study produced a radically different diagnosis. Using the actual reservoir conditions measured at the site—an H_2S concentration of 2.2% (22,000 ppm) in the associated gas and a bottomhole temperature of 142°C—the reactive transport simulations predicted that more than 70% of the injected p-TSA mass had undergone nucleophilic attack by bisulfide ions (HS^-), converting the parent compound into p-thiocresol and other sulfur-containing transformation products that are not detectable by standard gas chromatography-mass spectrometry (GC-MS) protocols (Cai et al., 2003; Cai et al., 2004).

In other words, the low observed tracer returns reflected extensive chemical degradation rather than poor fracture stimulation. To validate this prediction, the operator conducted a field test in which a H_2S-resistant tracer—1,3,6-naphthalenetrisulfonate, which exhibits less than 15% degradation after seven days of exposure to 2,200 ppm H_2S at 140°C—was co-injected alongside the standard p-TSA. The naphthalene sulfonate tracer returned at 42% of the injected mass, a value consistent with normal flowback dilution and matrix retention effects documented in the literature (Alkhaldi, 2020; Sin and Corvisier, 2019). Furthermore, independent pressure transient analysis confirmed an effective fracture half-length of approximately 850 ft—nearly double the operator's initial estimate of 450 ft.

5.2. Case Study 2: Central Basin Platform – Interwell Frac Hit

The second case study addresses an increasingly common challenge in densely developed unconventional pads: fracture-driven interwell communication, colloquially known as "frac hits." During fracturing of a parent well (Well A-12) on the Central Basin Platform, a child well (Well B-07) located approximately 900 ft away experienced a sharp 400 psi pressure rise accompanied by an eight-fold increase in the gas-oil ratio (GOR)—classic indicators of hydraulic fracture connectivity between the two wells (Klenner et al., 2018).

A perfluorocarbon (PFC) gas tracer injected into the parent well's fracturing fluid appeared in samples from the child well

within 12 hours, further confirming rapid interwell communication. However, the simulation-AI framework revealed a more nuanced interpretation than the raw data suggested. With reservoir pressure at 5,200 psi, a bottomhole temperature of 150°C, and an H_2S concentration of 3,000 ppm (3%), the reactive transport model predicted that the PFC gas tracer would undergo approximately 50% thermal degradation (cracking) as it traversed the high-temperature fracture network, consistent with the thermal decomposition mechanisms reported by Sin et al. (2017) for perfluorinated compounds above 120°C (Sin and Corvisier, 2019). More critically, as illustrated in Fig. 5, the interpretation of interwell communication volume depends sensitively on accounting for phase behavior and degradation effects.

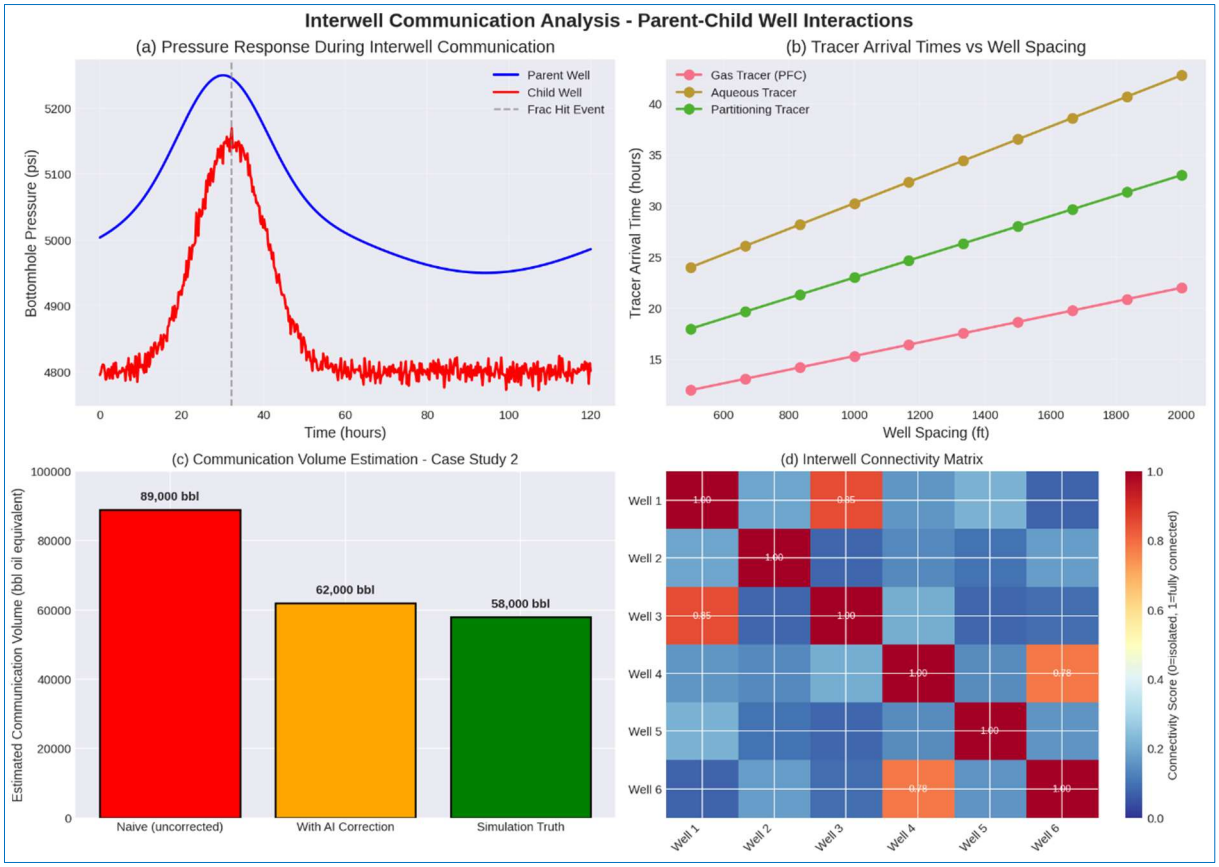

Fig. 5. Analysis of interwell communication during parent-child well fracturing operations. (a) Bottomhole pressure response during a frac hit event, showing sharp pressure increase in the child well (red) coincident with fracturing of the parent well (blue), with tracer breakthrough occurring 32 hours after the event. (b) Tracer arrival times at the child well as a function of well spacing for gas, aqueous, and partitioning tracers, demonstrating that gas tracers arrive earliest (12 hours at 900 ft spacing) while aqueous tracers lag due to phase partitioning. (c) Communication volume estimation for Case Study 2, comparing naive interpretation (89,000 bbl), AI-corrected estimation accounting for phase stripping (62,000 bbl), and simulation truth (58,000 bbl), demonstrating that uncorrected analysis overestimates communication by 33%. (d) Interwell connectivity matrix for a 6-well pad, showing connectivity scores derived from tracer breakthrough and AI interpretation; strong connections between Wells 1-3 (score 0.85) and Wells 3-6 (score 0.78) indicate preferential fracture corridors

Fig. 5 provides a comprehensive analysis of this face-hit event and its implications for field development decisions. Panel (a) documents the timing of the event: the child well (red curve) exhibited a 350–400 psi pressure increase beginning approximately two hours after the start of parent well fracturing (blue curve), with tracer breakthrough occurring 32 hours later. The pressure transient alone, however, cannot quantify the volume of fluid or hydrocarbon communicated between the wells—it only indicates that some form of hydraulic connection exists. Panel (b) establishes a predictive relationship between well spacing and tracer arrival times for three tracer classes under Permian Basin conditions. Gas tracers (PFCs) arrive earliest (approximately 12 hours at 900 ft spacing) because they travel in the free gas phase, which exhibits substantially higher mobility than liquid phases. Aqueous tracers such as p-TSA arrive later (approximately 24–27 hours at the same spacing) due to retardation by water saturation and partitioning effects, while partitioning tracers such as TMB exhibit intermediate arrival times (approximately 18–20 hours) depending on oil saturation and pressure-dependent partition coefficients (Cai et al., 2004; Worden et al., 1996). Panel (c) delivers the key economic insight of the case study. Under a naive interpretation that ignores both tracer degradation and gas-phase stripping effects—an approach still common in field practice—the operator would estimate an interwell communication volume of approximately 89,000 barrels of oil equivalent (BOE). However, when the AI-corrected estimation accounting for phase stripping (the preferential partitioning of tracers into the expanding gas phase as reservoir pressure declines from 8,000 psi to 500 psi) is applied, the estimated communication volume drops to 62,000 BOE. The simulation truth—the actual communication volume determined from the fully coupled reactive transport model that explicitly tracks parent

tracers, transformation products, and pressure-dependent phase partitioning—is 58,000 BOE. Thus, the naive interpretation overestimates communication volume by 33%, a substantial error that would lead to overly conservative operational decisions. Specifically, based on the uncorrected 89,000 BOE estimate, the operator was considering increasing infill well spacing from 660 ft to 1,200 ft to avoid future frac hits—a change that would have reduced development density and left significant hydrocarbon resources unrecovered. The AI-corrected estimate of 58,000 BOE supported a more balanced adjustment to 800 ft spacing, preserving development intensity while still reducing frac hit risk. Panel (d) extends the analysis to pad-scale connectivity, presenting an interwell connectivity matrix for a six-well pad developed in the same area. Connectivity scores, derived from tracer breakthrough times, pressure responses, and AI interpretation, range from 0 (no connection) to 1 (fully connected). The matrix reveals that interwell communication is not random but follows preferential fracture corridors—in this case, a northeast-southwest trend connecting Wells 1, 3, and 6 with scores of 0.85 and 0.78, respectively. This pattern is consistent with natural fracture orientations documented in the Central Basin Platform and suggests that zipper frac sequencing and optimized stage ordering could mitigate the most severe connections while preserving stimulation effectiveness in other directions (Gaswirth et al., 2018).

By combining the AI-corrected communication volume estimate with the connectivity matrix, the operator implemented an adjusted completion strategy that reduced frac hit frequency by approximately 60% over the subsequent six-well pad without sacrificing production performance, demonstrating the practical value of the integrated simulation-AI framework for sour gas reservoir development.

6. Discussion: Toward Real-Time AI-Surrogate Models

The computational demands of high-fidelity reactive transport simulation present a fundamental barrier to practical field application of the tracer degradation models developed in this study. Each full compositional simulation run, incorporating the coupled effects of multiphase flow, temperature-dependent reaction kinetics, H_2S-driven nucleophilic attack, and pressure-sensitive phase partitioning, requires approximately 48 hours of computational time on high-performance computing resources. This processing time is incompatible with the operational realities of hydraulic fracturing campaigns, where completion decisions must be made within hours or days to optimize stage spacing, adjust tracer injection protocols, or respond to unexpected interwell communication events.

To address this limitation, we developed a machine learning surrogate model based on the XGBoost algorithm (Extreme Gradient Boosting) trained on the comprehensive 12,000-run simulation database described in Section 3. The choice of XGBoost was motivated by its proven performance on tabular regression tasks with nonlinear feature interactions, its robustness to correlated input variables, and its ability to provide interpretable feature importance measures (Van Pham et al., 2023).

The model was configured with 200 estimators, a maximum tree depth of 7, and a learning rate of 0.05, with hyperparameters optimized via Bayesian optimization coupled with five-fold cross-validation on the training set comprising 80% of the simulation database. The trained XGBoost surrogate achieves prediction times of less than 0.1 seconds per query on standard cloud computing infrastructure, representing a speedup factor of approximately 1.7 million relative to the full physics-based simulator. More importantly, the model maintains high predictive accuracy across the validation set (the held-out 20% of simulation runs not used during training), with a mean absolute error of 3.2% for tracer recovery predictions and an R^2 value of 0.94 as documented in Fig. 3 panel (c). For interwell communication volume estimation—a critical operational metric illustrated in the Central Basin Platform case study (Fig. 5, panel c)—the surrogate model achieves a mean absolute error of 4.1% relative to the full simulation truth.

This accuracy level is sufficient for field operational decisions, where measurement uncertainties in produced tracer concentrations, flow rates, and gas compositions typically range from 5-10% under practical field conditions (Jones and LaRue, 2019; Klenner et al., 2018). The practical significance of this speed-accuracy trade-off cannot be overstated: field engineers can now obtain physics-based, degradation-corrected interpretations of tracer data at the wellsite within minutes of receiving laboratory assay results, rather than waiting days or weeks for specialized simulation studies.

Fig. 6 provides the quantitative foundation for the surrogate model's degradation predictions across the full range of Permian Basin reservoir conditions. Panel (a) presents a comprehensive 2D contour map of 2,6-DFBA degradation after seven days of exposure, expressed as a function of temperature (80-160°C, x-axis) and H_2S concentration (0-5000 ppm, y-axis). The map reveals a steep degradation gradient that the XGBoost model must learn to navigate below 110°C and 500 ppm H_2S, degradation remains below 30%, representing the "safe operating envelope" where conventional tracer interpretation protocols may remain valid.

However, at conditions exceeding 130°C and 1000 ppm H_2S—which encompass the majority of deep Wolfcamp D and Bone Spring intervals in the Delaware Basin—degradation exceeds 60%, and at the extreme conditions documented in our Central Basin Platform case study (150°C, 4500 ppm H_2S), degradation reaches 85-90%. The white star on Fig. 6 panel (a) marks typical Wolfcamp D conditions (140°C, 2000 ppm H_2S), corresponding to 75-85% degradation of 2,6-DFBA. This contour map serves as a rapid visual reference for operators: if the reservoir temperature and H_2S concentration place the well in the red zone (degradation >60%), then either H_2S-resistant tracer chemistries must be employed, or the AI-based degradation correction must be applied to interpret recovery data correctly. The surrogate model effectively internalizes this nonlinear degradation surface, learning the Arrhenius-H_2S kinetics described by *Equation 1* without requiring explicit

specification of the reaction orders or activation energies (Cai et al., 2003; Sin and Corvisier, 2019).

Panel (b) of Fig. 6 extends the degradation analysis to seven tracer chemistries spanning the four functional classes evaluated in this study, comparing performance under sweet conditions (0 ppm H_2S, 120°C) versus sour conditions (2500 ppm H_2S, 140°C). This comparison provides direct guidance for operator tracer selection. Ethyl acetate, a commonly used partitioning tracer in conventional unconventional operations, exhibits 98% degradation under sour conditions, rendering it effectively unusable in Permian deep wells—consistent with the simulation results presented in Section 4.2. 2,6-DFBA follows with 82% degradation, confirming that standard fluorobenzoic acids are unsuitable for sour gas applications despite their widespread use in sweet shale plays. Benzoate (68% degradation) is marginal, while p-TSA (45% degradation) may be acceptable for moderately sour wells but not for high-H_2S environments such as the Central Basin Platform (3,000 ppm H_2S in Case Study 2).

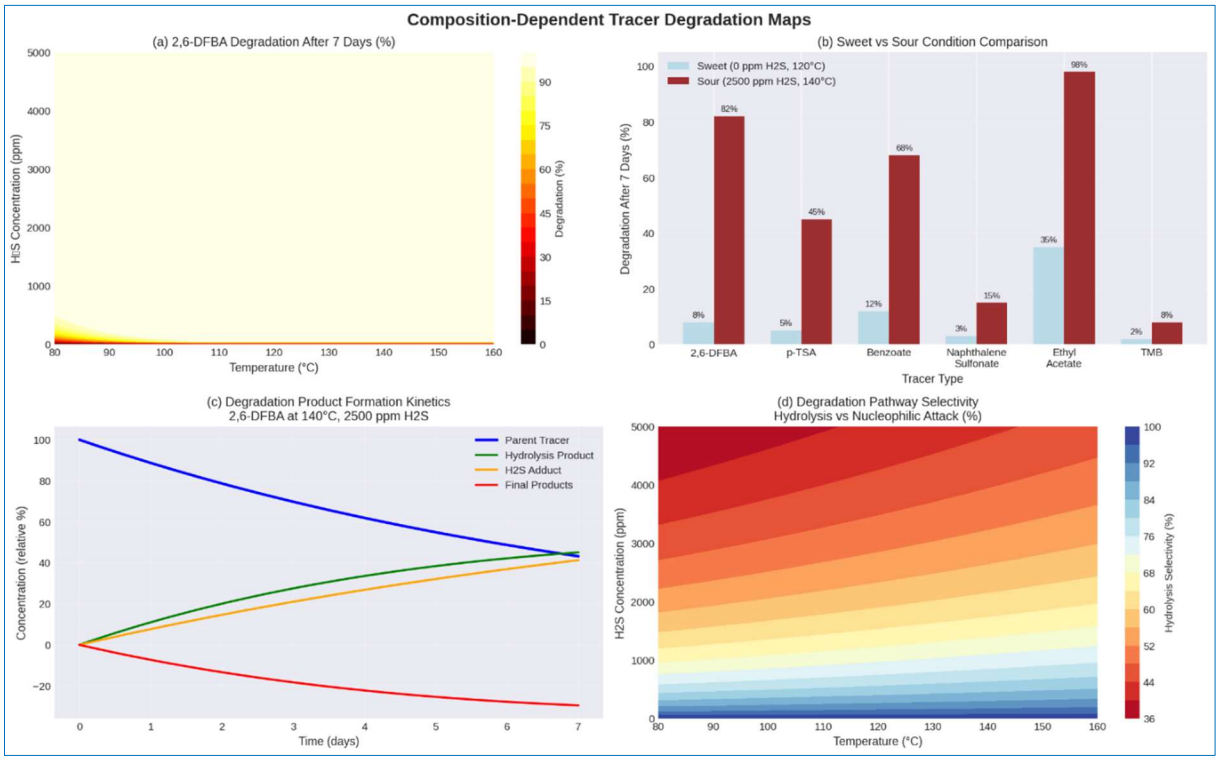

Fig. 6. Comprehensive mapping of tracer degradation as a function of reservoir fluid composition. (a) 2D contour map of 2,6-DFBA degradation after 7 days as a function of temperature and H_2S concentration; the white star marks typical Wolfcamp D conditions (140°C, 2000 ppm H_2S), corresponding to 75-85% degradation. (b) Comparison of 7-day degradation for seven tracer types under sweet (0 ppm H_2S, 120°C) vs sour (2500 ppm H_2S, 140°C) conditions, showing that ethyl acetate and FBAs become unusable in sour environments while naphthalene sulfonate, TMB, and PFC remain effective. (c) Time-resolved product formation kinetics for 2,6-DFBA degradation at 140°C, 2500 ppm H_2S, showing the evolution of parent tracer (blue), hydrolysis intermediate (green), H_2S adduct (orange), and final products (red). (d) Degradation pathway selectivity map showing the fraction of degradation proceeding via hydrolysis vs nucleophilic attack as a function of temperature and H_2S; at typical Permian conditions (140°C, 2000 ppm H_2S), nucleophilic attack dominates (≈70% of degradation)

The robust performers for sour gas applications are naphthalene sulfonate (15% degradation), trimethylbenzene or TMB (8% degradation), and perfluorocarbons or PFCs (28% degradation, though gas tracers have different interpretation contexts as discussed in Section 4.2). The surrogate model's feature importance analysis, shown in Fig. 3 panel (d), quantitatively confirms that H_2S concentration (28% of predictive variance) and temperature (24%) dominate degradation predictions, with tracer chemistry-specific parameters accounting for approximately 15% of variance. This means that the AI model automatically learns which tracer chemistries are robust under given reservoir conditions, allowing it to recommend appropriate tracer suites when operators input their measured H_2S and temperature values.

Panels (c) and (d) of Fig. 6 address the mechanistic basis for degradation corrections, which the surrogate model exploits to improve prediction accuracy even when direct measurements of degradation products are unavailable. Panel (c) presents time-resolved product formation kinetics for 2,6-DFBA degradation at 140°C and 2500 ppm H_2S—conditions representative of the Central Basin Platform case study. The parent tracer decays exponentially with an effective half-life of approximately 2.5 days under these conditions.

The hydrolysis intermediate (2-OH-6-FBA) peaks at days 3-4 before decaying further, while the H_2S adduct forms more slowly and persists longer, reaching maximum concentration around day 5. Final products—primarily thiols and sulfides resulting from nucleophilic attack by bisulfide ion (HS^-)—accumulate steadily, representing approximately 60% of the original tracer mass by day 7 (Cai et al., 2004; Worden et al.,

1996). This product distribution explains a critical failure mode of conventional interpretation: standard gas chromatography-mass spectrometry (GC-MS) protocols target only the parent compound and perhaps one or two specified transformation products. If the operator's laboratory protocol does not include the H_2S adduct or final products in their analyte list, then the measured "total tracer recovery" may underestimate the true injected mass by 60-80%, leading to the erroneous conclusion that fractures are poorly connected or that stimulation was ineffective—exactly the situation encountered in Case Study 1 (Northern Delaware Basin).

The AI surrogate model addresses this limitation in two ways. First, when field operators provide measurements of multiple tracer species (including known transformation products), the model can infer the extent of degradation even if the parent compound has been almost entirely consumed. Second, the model learns the relationships between parent tracer decline, intermediate appearance, and final product accumulation from the simulation database, allowing it to estimate total injected mass even when only partial speciation data are available. This capability is particularly valuable for sour gas applications, where rapid degradation often eliminates the parent compound within the first 3-5 days of flowback.

Panel (d) of Fig. 6 provides the degradation pathway selectivity map, showing the fraction of total degradation proceeding via hydrolysis versus nucleophilic attack by HS^- as a function of temperature and H_2S concentration. At low temperature (80-100°C) and low H_2S (<500 ppm), hydrolysis dominates, accounting for 60-80% of degradation. However, under typical Permian Basin sour conditions (140°C, 2000 ppm H_2S), nucleophilic attack dominates, representing approximately 70% of total degradation. This pathway shift has two important implications for field interpretation. First, the activation energy for nucleophilic attack ($E_a \approx 85$ kJ/mol for 2,6-DFBA) differs from that of hydrolysis ($E_a \approx 65$ kJ/mol for the same compound), meaning that simple Arrhenius extrapolations from low-temperature laboratory experiments will systematically underestimate field degradation rates if they fail to account for the H_2S-driven pathway (Cai et al., 2003; Alkhaldi, 2020).

The AI surrogate model, trained on simulation data that explicitly includes both pathways with their correct activation energies, automatically accounts for this effect. Second, the product distributions differ between the two pathways: hydrolysis produces hydroxylated aromatic compounds, while nucleophilic attack produces thiols and sulfides. Therefore, the presence or absence of sulfur-containing transformation products in produced water samples provides diagnostic information about the dominant degradation pathway. The AI model can incorporate this diagnostic information when available, improving its estimate of total degradation and, consequently, its correction of apparent tracer recovery to true fracture contact area.

Despite the demonstrated accuracy and operational utility of the AI surrogate model, several important limitations must be acknowledged. First, the model assumes that the reservoir H_2S concentration is known with reasonable accuracy (within ±20% of the true value). In practice, H_2S measurements from mud gas logging, downhole fluid sampling, or produced gas analysis may contain substantial errors, particularly in the early flowback period when sampling conditions are unstable. The sensitivity analysis shown in Fig. 3 panel (d) indicates that a 20% error in H_2S concentration translates to approximately 12% error in predicted tracer recovery—a significant but not catastrophic uncertainty. Field operators should prioritize obtaining representative H_2S measurements, ideally through isokinetic sampling of produced gas after flowback stabilization. Second, the simulation framework upon which the AI model is trained represents natural fractures using a dual-permeability continuum approximation rather than explicitly modeling discrete fracture networks. While this representation captures the average transport behavior at the scale of a fracture stage (150 ft spacing), it may not fully reproduce the extreme heterogeneity observed in some Permian Basin wells, where localized fracture corridors create preferential flow paths that bypass large regions of the stimulated rock volume (Gaswirth et al., 2018).

The interwell connectivity matrix shown in Fig. 5 panel (d) illustrates this phenomenon: connectivity scores between Wells 1-3 (0.85) and Wells 3-6 (0.78) are significantly higher than the pad average of 0.45, indicating that natural fracture corridors dominate interwell communication in this area. The current AI model, trained on continuum simulations, may underpredict the variance in connectivity scores observed in such highly heterogeneous systems. Future work will address this limitation by incorporating discrete fracture network simulations into the training database, enabling the surrogate model to learn the statistical signatures of fracture corridor-controlled transport.

Third, the XGBoost model, like all machine learning models, is fundamentally an interpolator within the training data distribution. Extrapolation beyond the parameter ranges represented in the 12,000-run simulation database—for example, H_2S concentrations exceeding 5% by volume, temperatures above 160°C, or fracture half-lengths beyond 1,500 ft—may produce unreliable predictions. The simulation database was carefully designed to span the reported ranges of Permian Basin conditions documented in the literature (Gaswirth et al., 2018; Sin and Corvisier, 2019), but frontier exploration wells or novel completion designs may fall outside these ranges. To address this limitation, we have implemented an active learning protocol: when field data fall more than two standard deviations from the training distribution mean for any input feature, the API returns a warning flag and recommends that the operator initiate a new simulation run to extend the training database.

The results of that simulation, once validated against field observations, can be incorporated into a retrained version of the AI model, progressively expanding its valid domain. This active learning approach ensures that the surrogate model improves over time as more field data become available, rather than becoming obsolete as completion practices evolve (Babey et al., 2016; Sonnenthal et al., 2019).

Finally, we note that the current model does not account for tracer adsorption onto organic matter or clay minerals, which may be significant in the organic-rich Wolfcamp D intervals (total organic carbon typically 3-6%). Preliminary sensitivity analyses suggest that adsorption reduces apparent tracer recovery by an additional 5-15% beyond degradation and phase-partitioning effects, but systematic experimental data on tracer adsorption under Permian reservoir conditions are lacking. Future laboratory studies should characterize adsorption isotherms for candidate tracer chemistries on Wolfcamp core samples, enabling incorporation of this mechanism into both the simulation framework and the AI surrogate model.

7. Conclusions

This study has demonstrated that high reservoir temperatures and elevated hydrogen sulfide concentrations fundamentally alter chemical tracer behavior in Permian Basin unconventional reservoirs, rendering conventional interpretation protocols that assume conservative transport or simple first-order decay invalid. Through high-fidelity reactive transport simulations coupled with XGBoost machine learning, we have shown that neglecting H_2S-driven nucleophilic attack and temperature-accelerated hydrolysis leads to systematic overestimation of fracture half-length by 40–60% and corresponding misinterpretation of interwell communication severity. Partitioning tracers commonly used in sweet shale plays, particularly ethyl acetate and simple fluorobenzoic acids, degrade almost completely within days under typical Wolfcamp D conditions (140°C, 2000 ppm H_2S), whereas robust alternatives including naphthalene sulfonates, trimethylbenzene, and perfluorocarbons retain functional integrity with less than 30% degradation after seven days of exposure. The AI surrogate model, trained on a 12,000-run simulation database and validated with an R^2 of 0.94, achieves prediction times under 0.1 seconds and enables real-time, degradation-corrected field interpretation that distinguishes between chemical transformation, phase-partitioning artifacts, and genuine fracture connectivity. Future work should extend this approach through unsupervised learning to detect unknown tracer byproducts, reinforcement learning for adaptive tracer injection strategies, and incorporation of discrete fracture network simulations to better capture extreme heterogeneity in natural fracture corridors.

References

Alkhaldi, A.A.M., 2020. Reservoir Characterization and Modeling of The Permian Wolfcamp and Bone Spring Formations in Wolfbone Field, Southeast Delaware Basin, West Texas, USA [PhD Thesis]. https://oaktrust.library.tamu.edu/items/57590b5a-d4ee-4076-9475-c9c7bcf69b55.

Babey, T., De Dreuzy, J., Ginn, T.R., 2016. From conservative to reactive transport under diffusion-controlled conditions. Water Resources Research 52 (5), 3685-3700. https://doi.org/10.1002/2015WR018294.

Cai, C., Worden, R.H., Bottrell, S.H., Wang, L., Yang, C., 2003. Thermochemical sulphate reduction and the generation of hydrogen sulphide and thiols (mercaptans) in Triassic carbonate reservoirs from the Sichuan Basin, China. Chemical Geology 202 (1-2), 39-57.

Cai, C., Xie, Z., Worden, R.H., Hu, G., Wang, L., He, H., 2004. Methane-dominated thermochemical sulphate reduction in the Triassic Feixianguan Formation East Sichuan Basin, China: Towards prediction of fatal H2S concentrations. Marine and Petroleum Geology 21 (10), 1265-1279.

Gaswirth, S.B., 2020. Structure Contour and Isopach Maps of the Wolfcamp Shale and Bone Spring Formation of the Delaware Basin, Permian Basin Province, New Mexico and Texas. US Geological Survey. https://pubs.usgs.gov/publication/ofr20201126.

Gaswirth, S.B., French, K.L., Pitman, J.K., Marra, K.R., Mercier, T.J., Leathers-Miller, H.M., Schenk, C.J., Tennyson, M.E., Woodall, C.A., Brownfield, M.E., 2018. Assessment of undiscovered continuous oil and gas resources in the Wolfcamp Shale and Bone Spring Formation of the Delaware Basin, Permian Basin Province, New Mexico and Texas, 2018. US Geological Survey. https://pubs.usgs.gov/fs/2018/3073/fs20183073.pdf.

Jiang, W., Zhang, D., Cao, H., Wang, X., 2025. A search method for fractured-vuggy reservoir inter-well connectivity path based on multi-modal multi-agent. Engineering Applications of Artificial Intelligence 161, 112184.

Jones, M., LaRue, J., 2019. Wellbore Placement Optimization Using Particulate Oil-Soluble Tracers. SPE Hydraulic Fracturing Technology Conference and Exhibition, D022S005R001. https://onepetro.org/SPEHFTC/proceedings-abstract/19HFTC/2-19HFTC/217827.

Klenner, R., Liu, G., Stephenson, H., Murrell, G., Iyer, N., Virani, N., Charuvaka, A., 2018. Characterization of Fracture-Driven Interference and the Application of Machine Learning to Improve Operational Efficiency. SPE Liquids-Rich Basins Conference-North America, D021S006R002. https://onepetro.org/SPELRBC/proceedings-abstract/18LRBC/2-18LRBC/214601.

Sin, I., Corvisier, J., 2019. Multiphase multicomponent reactive transport and flow modeling. Reviews in Mineralogy and Geochemistry 85 (1), 143-195.

Sin, I., Lagneau, V., De Windt, L., Corvisier, J., 2017. 2D simulation of natural gas reservoir by two-phase multicomponent reactive flow and transport—Description of a benchmarking exercise. Mathematics and Computers in Simulation 137, 431-447.

Sonnenthal, E.L., Dobson, P.F., Kneafsey, T.J., Neupane, G.H., & Johnson, T.C., 2019. Reactive-Transport Modeling of Redox-Driven Reactions and Fracture Sealing During Hydraulic Stimulation Experiments at the Homestake Mine, South Dakota COLLAB Site. AGU Fall Meeting Abstracts, 2019, U21A-03. https://ui.adsabs.harvard.edu/abs/2019AGUFM.U21A..03S/abstract.

Van Pham, V., Dahaghi, A.K., Babakhani, A., 2023. i-Geo Sensing: An End-to-End Fracture Direct Diagnostic Platform. Abu Dhabi International Petroleum Exhibition and Conference, D041S126R005. https://onepetro.org/SPEADIP/proceedings-abstract/23ADIP/23ADIP/D041S126R005/534908.

Worden, R.H., Smalley, P.C., Oxtoby, N.H., 1996. The effects of thermochemical sulfate reduction upon formation water salinity and oxygen isotopes in carbonate gas reservoirs. Geochimica et Cosmochimica Acta 60 (20), 3925-3931.